

Characterisation of Flow Pattern in a Rotor Stator High Shear Mixer

A. Pacek,^a M. Baker,^b A. T. Utomo^a

^a*School of Chemical Engineering, University of Birmingham, B15 2TT Birmingham, UK*

^b*Unilever R&D Port Sunlight, Quarry Road East, CH63 3JW Bebington, Wirral, UK*

Abstract

The flow in a rotor-stator high shear mixer (Silverson) at different rotor speeds have been simulated in Fluent using sliding mesh method with standard k- ϵ turbulence models and verified using LDA. The flow rate through the stator holes was directly proportional to rotor speed and the maximum energy dissipation rates occurred in the stagnation points at the edge of the stator holes. The agreement between measurements and simulation was generally very good, but the maximum velocity of the jets emerging from stator holes was underpredicted and the flow number calculated from numerical simulations were lower than flow number obtained from LDA measurements. The energy balance based on LDA measurements indicated that 70% of the energy is dissipated in close proximity to the mixer head whereas the k- ϵ model predicted that 50% of the energy is dissipated in the rotor swept volume, 5% in the gap between rotor and stator, 8% in the walls of the holes and 16% in the jets.

Keywords: rotor stator mixer, flow field, energy dissipation, CFD, LDA

1. Introduction

Rotor-stator mixers are commonly used in fine chemicals, food, cosmetics and pharmaceuticals industries to blend miscible liquids of different viscosities, to disperse fine solid particles in viscous liquids and to form stable emulsions of immiscible liquids (Myers et al., 1999). The typical feature of these mixers is a narrow gap between the rotor and the stator whose width varies from 100 to 3000 μm (Karbstein and Schubert, 1995). Typically the rotor tip speeds are between 10 and 50 m/s creating a high shear rate in the gap ranging from 20,000 to 100,000 s^{-1} (Atiemo-Obeng and Calabrese, 2004). Therefore, these devices are also called high shear mixers and cover different geometries such as colloid mills, toothed-devices, axial-discharge and radial-discharge rotor stator mixers (Atiemo-Obeng and Calabrese, 2004).

Davies (1985) and Karbstein and Schubert (1995) investigated the emulsification of immiscible liquids in high shear mixers (Hurrel type) and postulated drops are broken by turbulent pressure fluctuation since simple shear can not break the drops when the viscosity ratio (μ_d / μ_c) is greater than about 4.5 (Grace, 1982). On the other hand, Myers et al. (1999) reported that drops/agglomerates are mainly broken by planar shear in the gap, although elongational shear and shear in the turbulent eddies smaller than Kolmogorov's length also play part in breakage process. Elongational shear is effective for breakage of high viscosity drops suspended in the low viscosity continuous phase, however, it is difficult to estimate its magnitude in the high shear mixers. The shear in the smallest eddies is only effective when the drop size is smaller than Kolmogorov microscale.

Calabrese et al. (2000) investigated drop breakage in a high shear mixer fitted with a slotted head and found that the reduction of the gap widths (increase of shear rate) leads to the increase of average drop size. Based on this observation they concluded that the large drops (in the inertial subrange) were broken by turbulent pressure fluctuation and very small drops (of the order of Kolmogorov scale) were broken by viscous forces. This mixed break-up mechanism is possible because drops produced in the rotor stator mixer are very close to the Kolmogorov microscale (Padron, 2005). Calabrese et al. (2002) also suggested that the impingement on the stator surfaces and the jets emanating from the stator slots may provide the predominant dispersion mechanism.

The relation between power number (Po) and Reynolds number (Re) in the radial-discharge rotor stator mixer is similar to that in a stirred vessel (Padron, 2001; Doucet et al, 2005). In laminar flow, Po is inversely proportional to Re and in fully turbulent flow it is practically constant. In turbulent flow, the gap width has little effect on the power draw and doubling the gap width reduced Po by 10% (Padron, 2001). Atiemo-Obeng and Calabrese (2004) suggested that the energy dissipation in turbulent flow is controlled by fluid impingement on stator slot surfaces or turbulence in the jets emerging from the stator slots since Po increased with the number of openings in the stator. In laminar flow, Po is relatively independent of stator geometry but it varies slightly with gap width.

2D numerical simulations of in-line rotor-stator mixer (IKA Works) were carried out by Calabrese et al. (2002) for standard ($\delta = 0.5$ mm) and enlarged ($\delta = 4$ mm) gaps with water as the working fluid. In the case of standard gap, jets were emerging from the stator slot as the fluid impinged on the leading edge of stator teeth with circulation and re-entrainments in stator slots. The LDA data showed both stronger jets and re-entrainment flows than indicated by numerical simulation. The simulation also showed that the shear in the gap was not a simple shear, but turbulent shear flow. In the case of enlarged gap, the impingement on the leading edge of stator teeth was much weaker resulting in a much lower turbulent kinetic energy. Therefore, for efficient mixing/dispersion it is necessary to have a narrow gap even if the shear in the gap is not a major contributor to the dispersion process (Calabrese et al., 2002).

Although Calabrese et al (2002) showed that the turbulence in the jets and fluid impingement on the stator play an important role in dispersion process, the major weakness of their work is two dimensional simulation of an inherently three dimensional process. In this study a full three dimension numerical simulation verified by LDA measurements of instantaneous velocity distribution was employed to investigate the flow pattern, the pumping capacity and the distribution of energy dissipation rate in a batch radial-discharge rotor stator mixer. The prediction of the distribution of energy dissipation rate enables the determination of the most intense mixing/dispersion regions in the batch rotor stator mixer and enables more accurate scaling-up.

2. Experimental

2.1. Experimental

The rotor stator mixer investigated in this work was a 4 LRT (Silverson, UK) with a built-in tachometer. The mixing head was placed in the centre of the unbaffled, flat-bottom and free-surface glass beaker of diameter 150 mm. The liquid height was equal to the tank diameter and the clearance was half of the liquid height (Figure 1). The working fluid was water kept at constant temperature of 20 ± 1 °C and the vessel was placed in a rectangular glass box also filled with water to minimize the refraction of laser beams due to the curvature of vessel wall. The rotor speed was varied from 2000 – 4000 rpm ($Re = 26,000 - 52,000$).

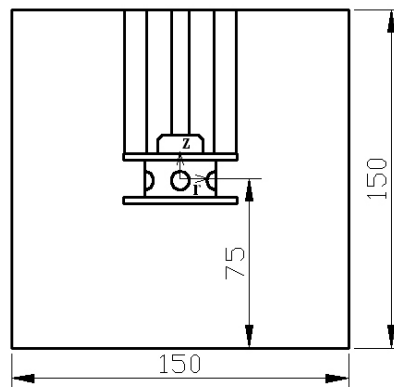


Figure 1: Position of the mixer in the tank (dimensions in mm).

The mixing head was fitted with standard disintegrating head/stator with 6 holes of 8 mm diameter shown in Figure 2 and 3. The stator diameter was 28.2 mm and the gap width was 0.175 mm. The origin of r , z and θ coordinate system was located in the center of the shaft at the midpoint between upper and lower plates.

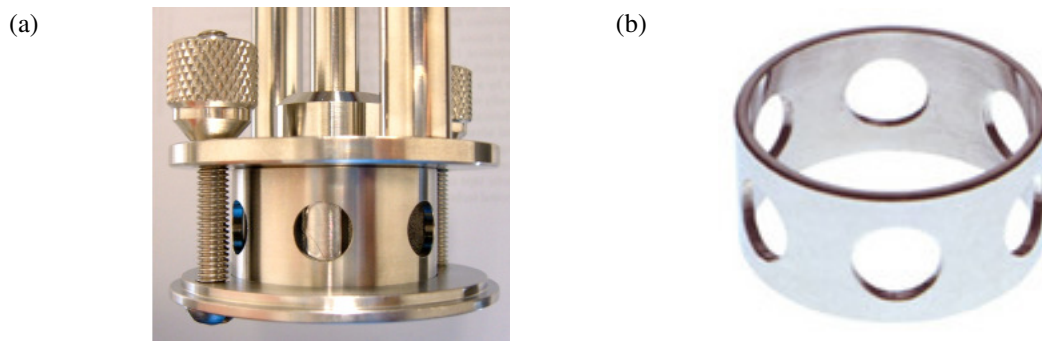


Figure 2 : Silverson mixing head (a) a rotor stator assembly, (b) a standard disintegrating head (from www.silverson.com).

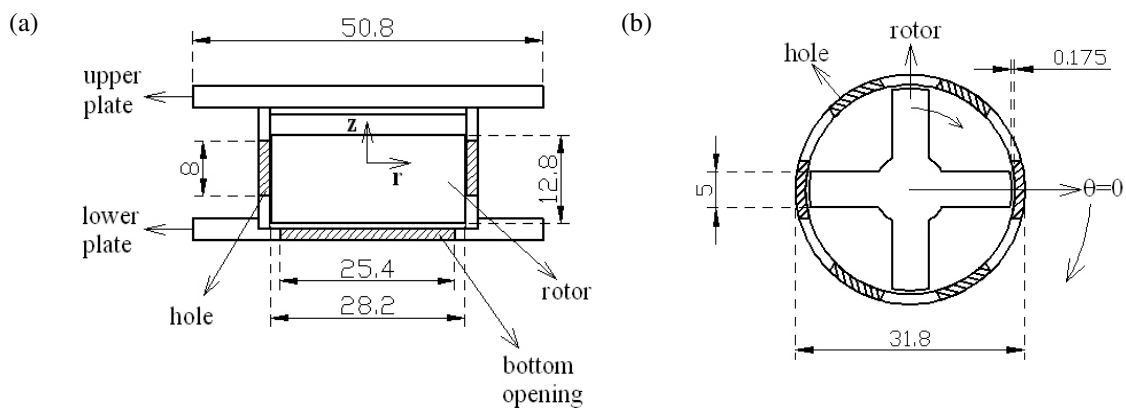


Figure 3 : Details of mixing head: (a) vertical cross section and (b) horizontal cross section. The rotor rotates in clock-wise direction as viewed from the above and θ is positive in the clock-wise direction (dimensions in mm).

A LDA system operating in the backscatter mode (TSI) and allowing simultaneous measurements of 2 velocity components was used in this work. The properties of laser beams are shown in Table 1. The laser probe was mounted on the 3D computer-controlled traverse with an accuracy of 0.01 mm in each direction. Water was seeded with 10 μm silver coated, hollow glass sphere. The velocity in each point was represented as an ensemble average of instantaneous velocity. The number of data collected in each point was 30,000 in the bulk region and 50,000 in the vicinity of the stator for both axial and radial velocity which was well above the minimum of 6,000 data for good reproducibility as suggested by Zhou and Kresta (1996). The maximum acquisition time was 180 seconds and the actual acquisition time varied from 40 seconds to 120 seconds. The error in LDA measurements was between 3-5% of the tip velocity (Mishra et al., 1998).

Wavelength (λ)	514.5 nm (green)	488 nm (blue)
Half Angle (κ)	11.563°	11.563°
Fringe Spacing (d_f)	1.283 μm	1.213 μm
Focal Distance (f)	122.19 mm	122.19 mm
Diameter (d_m)	32.70 μm	31.01 μm
Length (l_m)	159.81 μm	157.91 μm

Table 1 : Properties of the laser beams and measurement volumes.

2.2. Mass and energy balances from LDA data

The mass and energy balances around the mixing head are set in a control volume shown in Figure 4. Boundary 1 is a horizontal circle, located 4 mm below the stator lower surface. Boundary 2 is a vertical cylindrical surface between boundary 1 and the bottom plate of the stator. Boundary 3 is the area of 6 vertical circles of the same diameter as the stator hole located 0.3 mm away from the hole. These boundaries are discretized into segments as shown in Figure 5. The fluid velocity was measured in the centre of each segment and the mass flow-rate through boundary i (Q_i) was calculated as

$$Q_i = \rho \sum a_{jk} U_{jk} \tag{1}$$

where a_{jk} is the area of segment jk and U_{jk} is the mean velocity component perpendicular to segment jk . In this calculation, the mass of fluid flowing into the control volume was taken as positive.

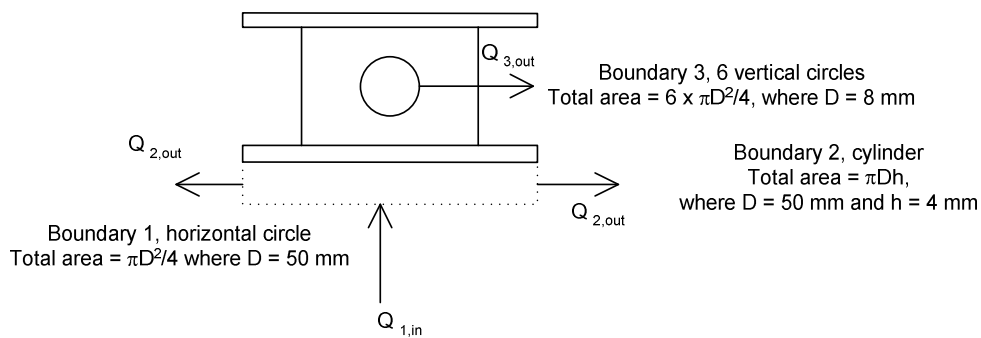


Figure 4 : The control volume around the mixing head for mass and energy balances.

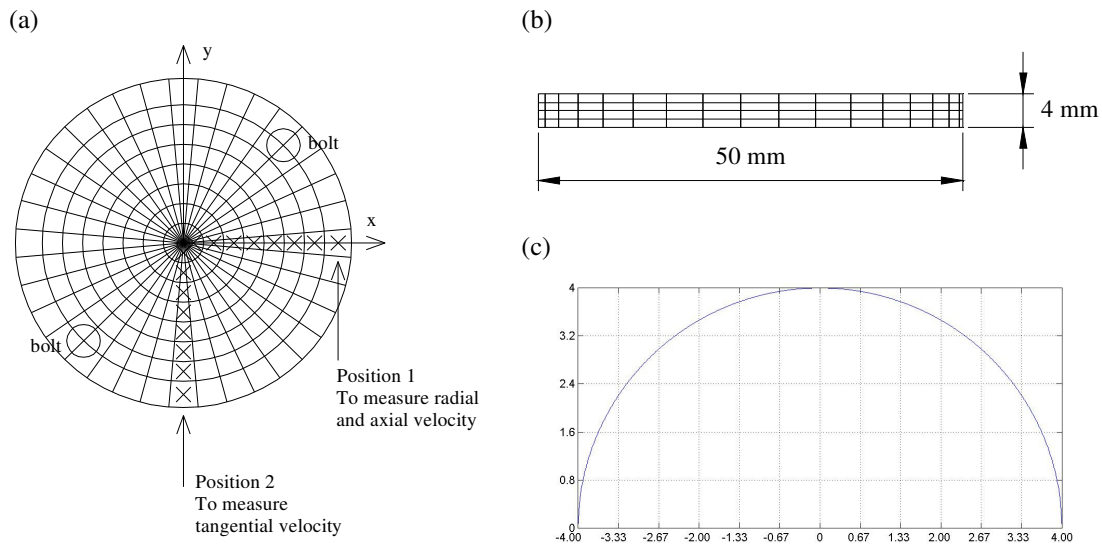


Figure 5 : (a) Boundary 1 is discretized by 8 concentric circles in the radial direction and 36 sections in the tangential direction; the crosses (x) show the points of measurements; (b) boundary 2 is discretized into 4 sections in axial direction and also 36 sections in tangential direction; (c) boundary 3 is discretized into 0.67 x 0.8 mm rectangulars.

The amount of energy dissipated in the control volume (E_{diss}) was calculated using total kinetic energy balance (Wu and Patterson, 1989; Zhou and Kresta, 1996):

$$E_{diss} = \sum E_{in} - \sum E_{out} = E_{rotor} + E_{K1} + E_{K2} + E_{K3} \quad (2)$$

where E_{rotor} is the energy transferred to the fluid by rotor

$$E_{rotor} = Po\rho N^3 D^5 \quad (3)$$

where Po is the rotor power number and was taken as 1.7 for standard disintegrating head (Padron, 2000), E_{K1} , E_{K2} and E_{K3} are the total kinetic energy rate through boundary 1, 2 and 3 respectively. In this energy balance, energy flows into the control volume was taken as positive. E_{K1} , E_{K2} and E_{K3} were calculated as the sum of the product of mass flowrate times the total kinetic energy

$$E_{Ki} = \frac{\rho}{2} \sum a_{jk} U_{jk} KE_{jk} \quad (4)$$

Where KE_{jk} is the total kinetic energy, defined as (Wu and Patterson, 1989)

$$KE_z = (U_z^2 + U_r^2 + U_\theta^2 + 3\overline{u_z'^2} + \overline{u_r'^2} + \overline{u_\theta'^2}) \quad (5)$$

$$KE_r = (U_z^2 + U_r^2 + U_\theta^2 + \overline{u_z'^2} + 3\overline{u_r'^2} + \overline{u_\theta'^2}) \quad (6)$$

2.3. Numerical Simulation

The numerical simulation was carried out using Fluent 6.2 and the following differential mass and momentum balances for incompressible fluid have been solved (Versteeg and Malalasekera, 1995):

$$\frac{\partial U_i}{\partial x_i} = 0 \quad (7)$$

$$\frac{\partial U_i}{\partial t} + U_j \frac{\partial U_i}{\partial x_j} = -\frac{1}{\rho} \frac{\partial P}{\partial x_i} + \nu \frac{\partial^2 U_i}{\partial x_j \partial x_j} - \frac{\partial \overline{u'_i u'_j}}{\partial x_j} \quad (8)$$

where U_i is the average velocity, P is the average pressure, ν is the kinematic viscosity and $\overline{u'_i u'_j}$ is the Reynolds stresses. In this simulation, standard k- ϵ turbulent model was used to solve those equations.

The computational model was a full 3-D geometry consisted of about 600,000 non-uniformly distributed hybrid cells (tetrahedral and hexahedral) in the bulk tank region and about 400,000 hybrid cells inside the rotor stator region (Figure 6). The gap between rotor and stator was divided into 5 hexahedral cells.

The simulation was started with steady state multiple reference frames and then continued with transient sliding mesh model. QUICK discretization scheme and enhanced wall function were used in the transient simulation. The interface between rotating and stationary regions was located in the middle of the gap. The time step in the transient sliding mesh model was 1/30 of the rotor revolution time. For transient simulation in stirred tank, with either RANS or LES, converged solution is usually obtained after 20 revolutions (Ng et al., 1999; Roussinova et al., 2003).

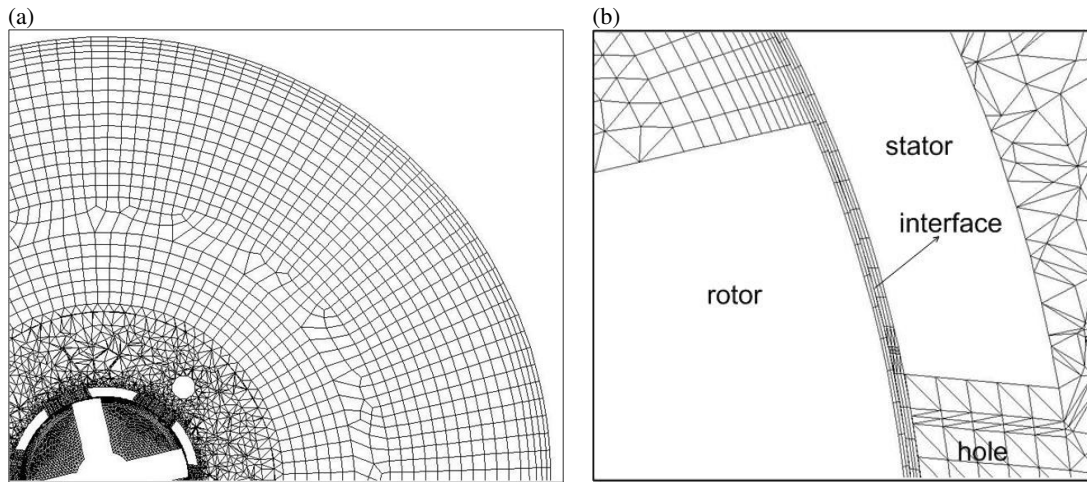


Figure 6: (a) Grids used in the simulation; (b) detail of the grids in the gap; the interface indicates the boundary between rotating and stationary mesh.

3. Result and Discussion

3.1. Flow pattern in the proximity of the jets

The predicted velocity vectors around the stator hole at various blade positions are shown in Figure 7(a) – (c). The jet emerging from the stator hole is due to the impingement of fluid on the leading edge of the stator hole wall which converts tangential velocity into radial velocity. The flow pattern around the stator hole is obviously affected by the position of the blade and the maximum velocity of the jet occurs when the blade is approaching the leading edge of the stator.

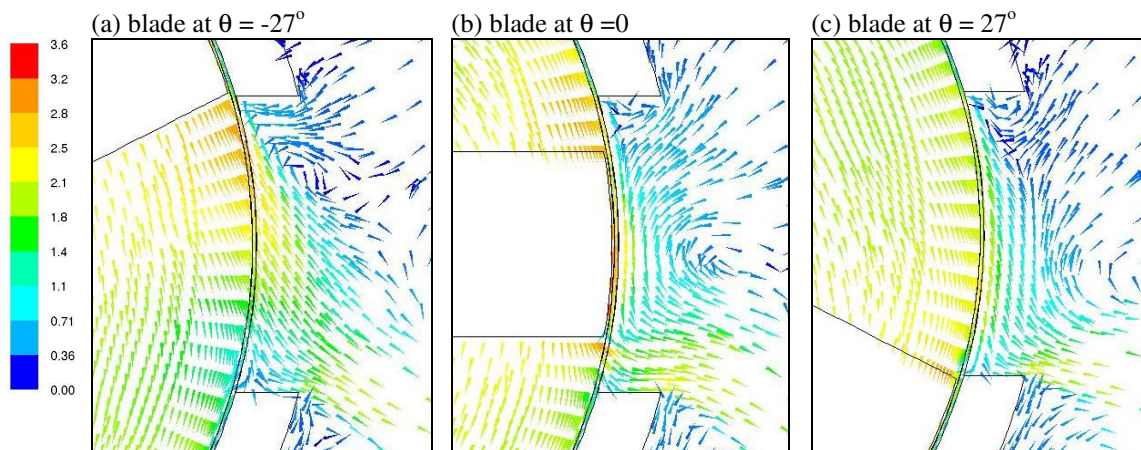


Figure 7 : Calculated velocity vectors (k- ϵ model, 2000 rpm) around the stator hole at $z = 0$, (a) blade at $\theta = -27^\circ$, (b) blade at $\theta = 0$, (c) blade at $\theta = 27^\circ$. All vectors have same length and their magnitudes are indicated by colour.

Just behind the jet, the liquid from the bulk flows towards the hole, but does not enter the rotor swept volume e.g. small circulation loop exist. This liquid merges with the liquid from rotor swept volume and is ejected as jet. The flow pattern is very similar to that reported by Calabrese et al. (2002) for in-line rotor stator mixer who also observed circulation behind the jet.

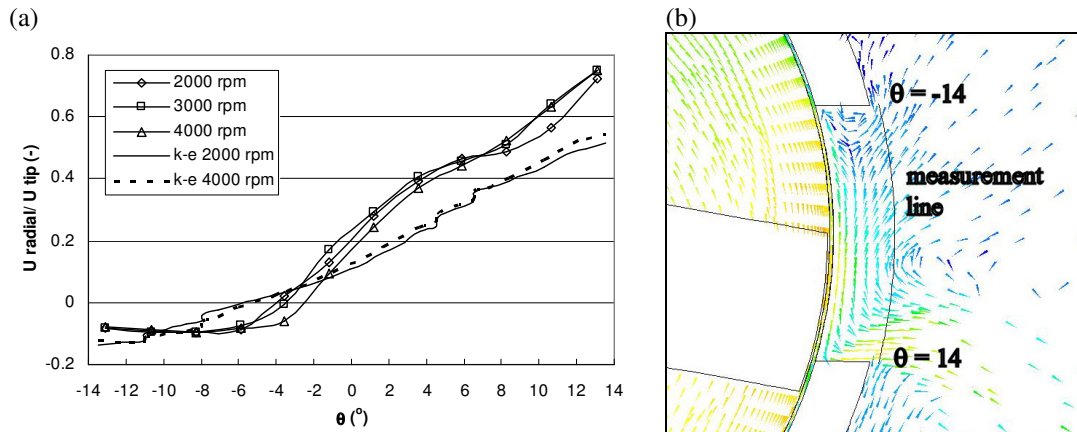


Figure 8 : (a) Comparison of the normalized (by tip speed) radial velocity profiles of the jet between LDA measurement and CFD prediction (positive direction is out of stator), (b) position of the measurement line.

Although the instantaneous velocity profile in the hole is affected by the position of the blade, the ensemble average of the instantaneous velocity across the center of the hole shows a certain kind of pattern. The comparison of the normalized radial velocity profile across the centre of the stator hole between LDA measurements and CFD simulations is shown in Figure 8(a). The LDA data shows that maximum radial velocity of the jet occurs at the leading edge of stator hole and the radial velocity decreases almost linearly with the distance from the leading edge until finally the velocity become zero and the liquid flows in the reverse direction with almost constant velocity. The k- ϵ model predicts the same trend as LDA measurement, but the maximum velocity is underpredicted by 25%. Both LDA data and CFD prediction shows that normalized radial velocity profiles falls into one line suggesting that the radial velocity is proportional to the rotor speed.

3.2. Flow pattern around the mixing head and in the bulk region

The velocity vectors around the mixing head and in the bulk region at plane $z = 0$ predicted with k- ϵ model are shown in Figure 9 (a) and (b) respectively. The flow pattern around the mixing head is rather complex due to the presence of high velocity jets and recirculation loops induced by those jets. The velocity in the jets is a few orders of magnitude higher than in other parts of the vessel. The jets emerging from the holes extend up to the tank wall with the radial velocity gradually decreasing and are converted back into tangential velocity by tank wall which create circulation in the bulk of the liquid. The tangential and radial components in the bulk are rather low therefore bulk mixing in the rotor/stator devices is not very intensive.

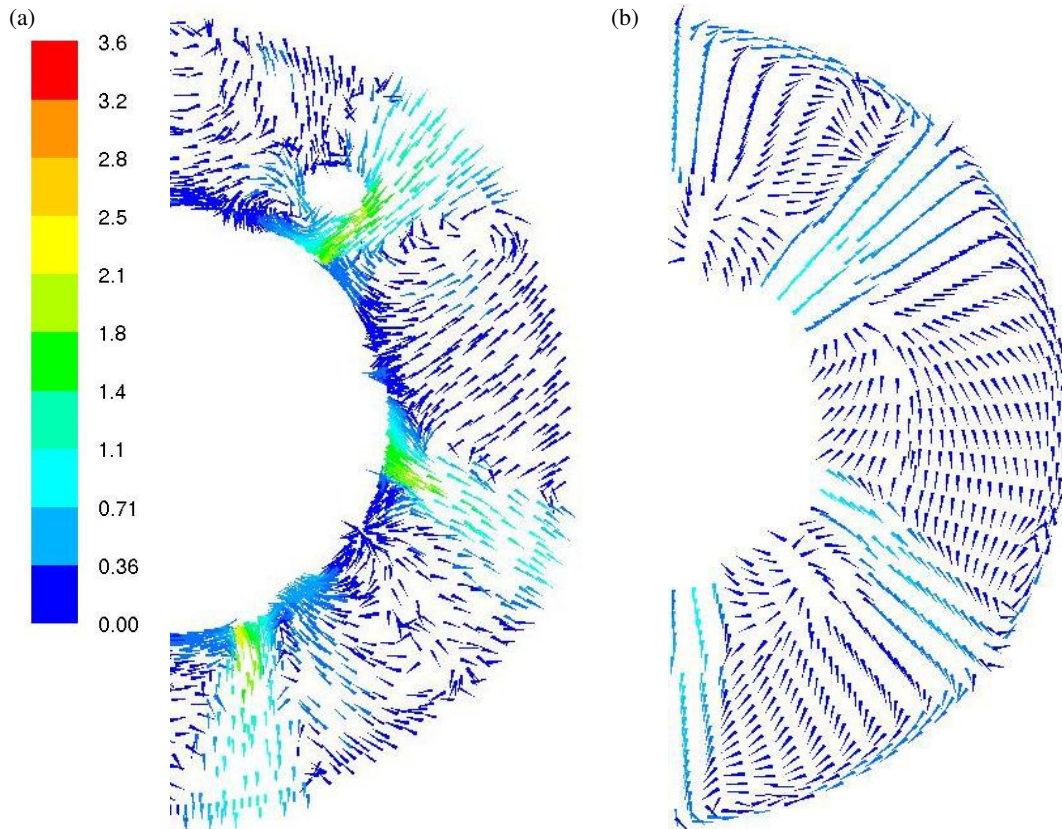


Figure 9 : Radial-tangential velocity vectors at plane $z = 0$ (2000 rpm) predicted by $k-\epsilon$ model, (a) around mixing head and (b) in the bulk region. All vectors have same length and their magnitudes are indicated by colour.

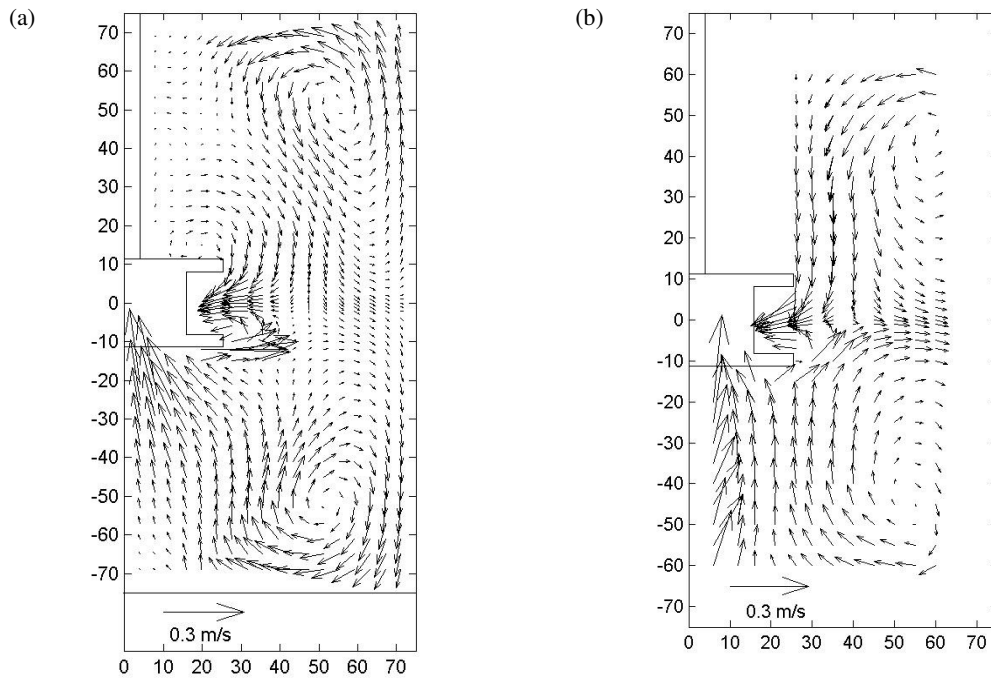


Figure 10 : Axial-radial velocity vectors at plane $\theta = 0$ (2000 rpm), (a) standard $k-\epsilon$ model and (b) LDA measurements.

The radial/axial velocity vectors at plane $\theta = 0$ predicted using k- ϵ model and measured using LDA are shown in Figure 10. The qualitative agreement between LDA measurement and simulation results is very good and in both cases circulation loops at the regions above and below the mixing head were detected. In the middle of the tank the liquid flows both towards the walls and the towards stator holes. As the plane $\theta = 0$ is located at the middle of the hole, the velocity vectors shown in this figure correspond to the fluid behind the jet and the velocity distribution in the jet itself is not captured. The more detailed comparison of calculated and measured velocity distributions are shown in Figure 11.

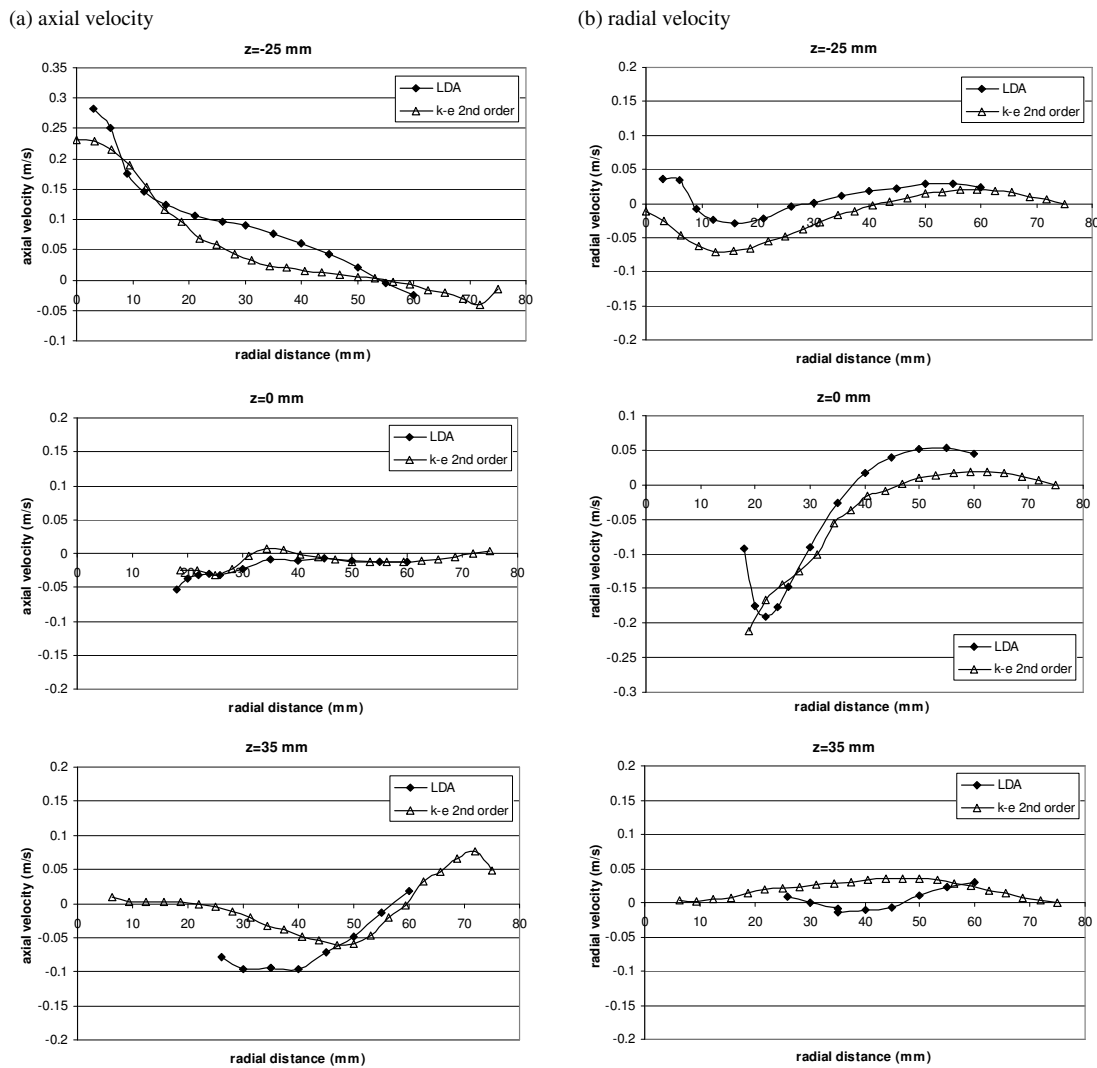


Figure 11: Comparison of axial and radial velocities obtained from LDA measurement and CFD simulations.

The above results clearly show that the flow both close the mixing head and in the bulk is fully 3D with axial and tangential velocity close to the mixing head of the similar order and radial velocity of the jets dominating the flow

3.3. Mass balance

The results of mass balances in the control volume shown in Figure 4 based on LDA data and CFD predictions at 2000 and 4000 rpm are summarised in Table 2 and Table 3 respectively. As expected, at both speeds, the mass balance based on the calculated velocity field is closed whereas there is a difference between inlet and outlet in the mass balances based on LDA data. The maximum difference between inlet and outlet does not exceed 5% which is a typical error band for a mass balance calculation based on LDA data (Wu and Patterson, 1989, Zhou and Kresta, 1996).

2000 rpm	LDA	k-ε model	Difference between LDA and CFD
Boundary 1	0.265 kg/s	0.243 kg/s	0.0215 kg/s (8.1%)
Boundary 2	-0.110 kg/s	-0.112 kg/s	0.0025 kg/s (2.3%)
Boundary 3	-0.158 kg/s	-0.131 kg/s	0.027 kg/s (17.1%)
Difference (%)	0.003 kg/s (1.1 %)	0 kg/s (0 %)	

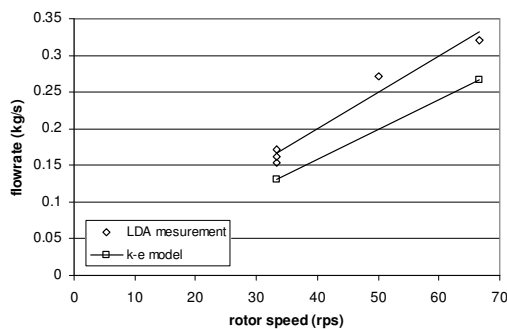
Table 2: Comparison of mass balances around mixing head based on LDA and CFD at 2000 rpm

4000 rpm	LDA	k-ε model	Difference between LDA and CFD
Boundary 1	0.600 kg/s	0.448 kg/s	0.152 kg/s (25.3%)
Boundary 2	-0.250 kg/s	-0.182 kg/s	0.068 kg/s (27.2%)
Boundary 3	-0.320 kg/s	-0.266 kg/s	0.054 kg/s (16.8%)
Difference (%)	-0.03 kg/s (5 %)	0 kg/s (0 %)	

Table 3 : Comparison of mass balances around mixing head based on LDA and CFD at 4000 rpm

The total flow-rate through the holes calculated both from LDA data and from CFD simulation is proportional to rotor speed with LDA giving marginally higher flow-rate as shown in Figure 12(a). Consequently the flow number ($Fl = Q/ND^3$) obtained from LDA measurement was 0.217, while that predicted by k-ε model was 0.176 (Figure 12 (b)).

(a)Flowrate through 6 holes vs rotor speed



(b)Flow number (Fl) vs rotor speed

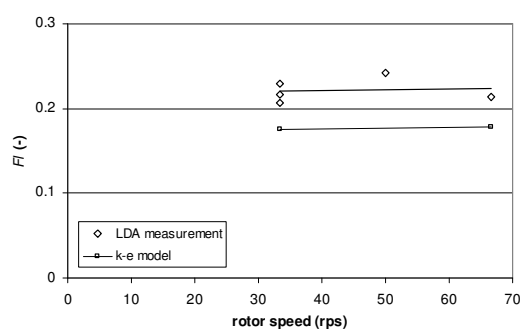


Figure 12 : (a) Flow-rate through holes against rotor speed; (b) Flow number against rotor speed.

The flow parameters for rotor stator mixer and Rushton turbine are compared in Table 4 where pumping efficiency, E_p , was calculated from (Bakker and Van den Akker, 1990)

$$E_p = \frac{Q^3 \rho}{PT^4} = \frac{Fl^3}{P_o} \left(\frac{D}{T} \right)^4 \quad (9)$$

The pumping efficiency of the rotor stator mixer is about two orders of magnitude lower than that of Rushton turbine. This again shows that the bulk mixing in the batch rotor stator mixer is very poor.

Impeller	D/T	Po	Fl	$E_p (10^{-6})$
Rotor stator	0.188	1.7	0.22	7.5
Rushton turbine	0.333	5	0.74	997

Table 4 : Comparison of flow parameters for rotor stator mixer and Rushton turbine (Nienow, 1997).

3.4. Energy dissipation rate

The solution of energy balance based on LDA data (Table 5) indicates that approximately 70% of energy supplied by rotor is dissipated inside the control volume defined in Figure 4 e.g. it accounts for the energy dissipated in the rotor swept volume, gap and in holes region (Figure 13). In turbulent flow, the energy dissipated in the control volume increases approximately 8 times when the rotor speed is doubled which indicates that energy dissipation is proportional to N^3 .

	2000 rpm	4000 rpm
$E_{rotor} (P_o \rho N^3 D^5)$	1.123 W	8.98 W
E_{K1}	0.063 W	0.713 W
E_{K2}	-0.015 W	-0.188 W
E_{K3}	-0.383 W	-3.029 W
E_{diss}	0.787 W	6.479 W
% energy dissipated/energy input	70.16 %	72.15 %
Average energy dissipation/unit mass ($\bar{\epsilon}$) in the control volume	48.9 m ² /s ³	402.2 m ² /s ³

Table 5 : Energy balance around the rotor stator head at 2000 and 4000 rpm.

At 2000 rpm, the simulation predicts that 50% of the energy is dissipated in the rotor swept volume and only 16% of energy is dissipated in the jet region (Figure 13 (a)). Although the total amount of energy dissipated in the whole tank predicted by k- ϵ model is only about 65% of the actual energy supplied by rotor, the percentage of energy dissipated in the control volume predicted by k- ϵ model is about 63% which is in a good agreement with the energy balance based on LDA data. The inaccuracy of k- ϵ model to predict the total amount of energy dissipation in mixing tank has been mentioned by several authors (Ng and Yianneskis, 2000; Yeoh et al., 2004). Nevertheless, Ng and Yianneskis (2000) used k- ϵ model to predict the distribution of energy dissipated in the baffled tank stirred by a Rushton turbine and got a good agreement with the experimental result from Zhou and Kresta (1996).

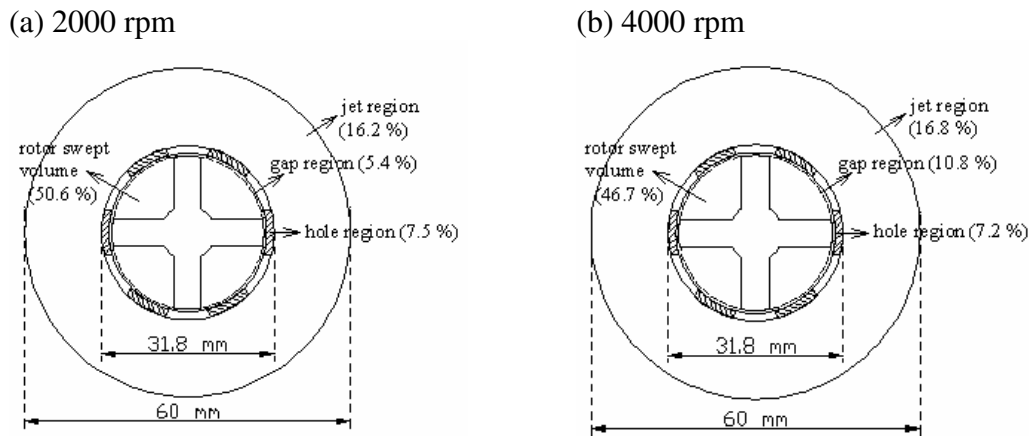


Figure 13 : Comparison of the distribution of the energy dissipation rate predicted by k-ε model at (a) 2000 rpm and (b) 4000 rpm. Jet region is defined as the annular region between stator outer diameter ($r = 15.9$ mm) and $r = 30$ mm.

The simulation also predicts that the energy dissipated in the gap increases from 5% at 2000 rpm to about 10% at 4000 rpm, whereas in the other regions, the percentages of energy dissipated are practically the same. This may suggest that the flow in the gap is turbulent flow whose intensity increases with rotor speed.

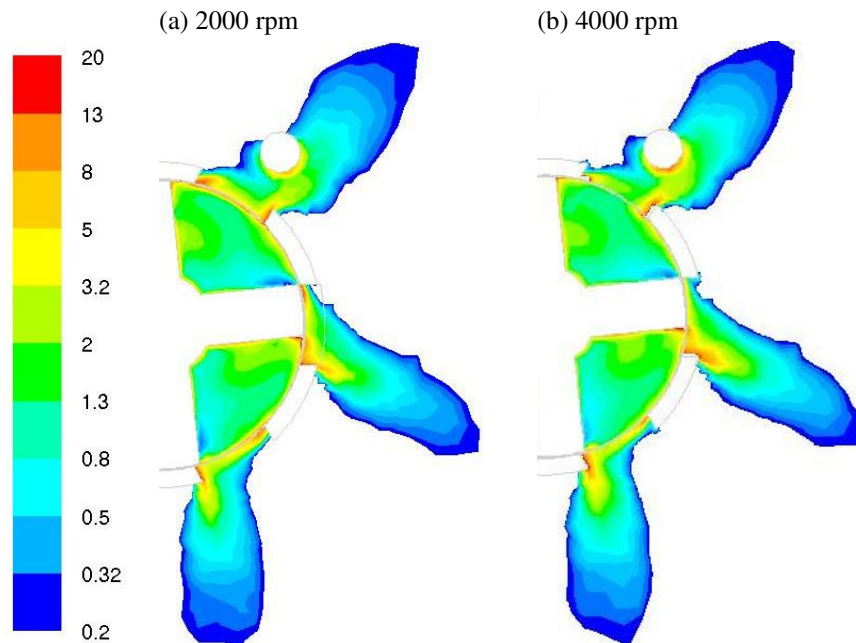


Figure 14: Comparison of the normalized contour of the energy dissipation rate (ϵ/N^3D^2) predicted by k-ε model at (a) 2000 rpm and (b) 4000 rpm.

The normalised (with respect to N^3D^2) contours of energy dissipation rate per unit mass (ϵ_{norm}) at 2000 rpm and 4000 rpm calculated using k-ε model are shown in Figure 14. From this figure it is clear that normalised energy dissipation rate is independent on rotor speed and the highest energy dissipation rate occurs at in the jet

at close to the leading edge of the hole when the rotor blade is approaching this edge. When the rotor blade overlaps with the leading edge, the ε decreases but remains much higher than energy dissipation in other point in the mixing head. The energy dissipation rate in the gap is smaller than in the impinging jets but larger than in the rotor swept volume.

The identification of the regions in the high shear mixer of different intensity of energy dissipation rate together with the knowledge of local flow rates in such regions can be used to predict the mechanisms of drop breakage in liquid/liquid or liquid/solid two phase systems.

4. Conclusions

The complex three dimensional flow in high shear mixer has been simulated using Fluent 6.2 with k- ε turbulent model and verified experimentally using LDA. In general the agreement between calculated and measured velocity field was very good. The results show the radial velocity of the jets and the flow-rate through stator holes are proportional to the rotor speed and that approximately 70% of the energy supplied by the rotor is dissipated in the proximity of mixing head. In turbulent flow the energy dissipation in this region is proportional to N^3 .

The CFD simulation predicts that about 50% of energy is dissipated in the rotor swept volume with the maximum energy dissipation occurring during the impingement of the fluid on the leading edges of the stator holes. The energy dissipated in this region is predicted to be only 7.5% of the total energy supplied. The highest energy dissipation rate during fluid impingement only occurs intermittently when the rotor blade approaches the leading edge of the stator hole. Therefore, it is important to have a very narrow gap to provide maximum kinetic energy to the fluid during impingement (Calabrese et al., 2002).

5. Acknowledgement

The financial support provided by Unilever R&D Port Sunlight and by The University of Birmingham is gratefully acknowledged.

6. Notation

D	diameter of rotor or boundary 1, 2, 3, m
E_{diss}	energy dissipation rate in control volume, J/s
E_{Ki}	kinetic energy flowrate in i direction, J/s
E_p	pumping efficiency
E_{rotor}	power supplied to liquid through rotor, J/s
E_{Tot}	total energy flowrate, J/s
KE_i	total kinetic energy in i direction, m^2/s^2

H	segment height in boundary 2, m
m	number of cells in tangential direction, -
n	number of cells in radial direction, -
N	rotation speed, 1/s
Fl	flow number, Q/ND^3
P_o	power number, $P/\rho N^3 D^5$
P	power, J/s or average pressure, Pa
Q_i	mass flowrate through surface i, kg/s
Re	Reynolds number, $\rho ND^2/\mu$
r_i	radial distance of cell i, m
u'_i	fluctuating velocity in i direction, m/s
U_i	mean velocity in i direction, m/s
W	blade width, m

Greek letters

δ	gap spacing, m
$\bar{\epsilon}$	average energy dissipation rate per unit mass, m^2/s^3
μ	viscosity, kg/m s
ν	kinematic viscosity, m^2/s
ρ	density, kg/m^3

Subscript

r	radial direction
z	axial direction
θ	tangential direction

7. References

- Atiemo-Obeng, V. A. and Calabrese, R. V., 2004. "Rotor-stator mixing devices" in *Handbook of Industrial Mixing: Science and Practice*, E. L. Paul, V. A. Atiemo-Obeng and S. M. Kresta, John Wiley & Sons, Hoboken, New Jersey, USA.
- Baldyga, J., Bourne, J. R., Pacek, A. W., Amanullah, A., and Nienow, A. W., 2001. "Effects of agitation and scale-up on drop size in turbulent dispersions: allowance of intermittency", *Chem. Eng. Sci.*, **56**: 3377 – 3385
- Bakker, A. and van den Akker, H. E. A., 1990. "The use of profiled axial flow impellers in gas-liquid reactors", *In Fluid Mixing IV, Inst. Chem. Engng. Symp. Ser. No. 121*, pp. 153 166.
- Calabrese, R. V., Francis, M. K., Mishra, V. P. and Phongikaroon, S., 2000. "Measurement and analysis of drop size in a batch rotor-stator mixer", *10th European Conference on Mixing*, H. E. A. van den Akker and J. J. Deksen, eds., Elsevier Science, Amsterdam, pp. 149-156.
- Calabrese, R. V., Francis, M. K., Kevala, K. R., Mishra, V. P., Padron, G. A. and Phongikaroon S., 2002. "Fluid dynamics and emulsification in high shear mixers", *Proc. 3rd World Congress on Emulsions*, Lyon, France, Sept.
- Davies, J. T., 1985. "Drop size distribution related to energy dissipation rates", *Chem. Eng. Sci.*, **40**: 839 – 842.
- Doucet, L., Ascanio, G. and Tanguy, P. A., 2005. "Hydrodynamics characterization of rotor-stator mixer with viscous fluids", *Trans. IChemE, Part A*, **83**: 1186-1195.
- Hinze, J. O., 1955. "Fundamentals of the hydrodynamics mechanism of splitting dispersion process", *A.I.Ch.E. Journal*, **1**: 289 – 295.

<http://www.silverson.com>

- Karbstein, H. and Schubert, H., 1995. "Development in continuous mechanical production of oil-in-water macro emulsions", *Chem. Eng. Process.*, **34**: 205 – 211.
- Mirsha, V. P., Dyster, K. N., Zaworski, Z., Nienow, A. W. and McKemmie, J., 1998. "A study of an up and a down pumping wide blade hydrofoil impeller: Part1. LDA measurement", *Can. J. Chem. Eng.*, **76**: 577 – 588.
- Myers, K. J., Reeder, M. F., Ryan, D., and Daly, G., 1999. "Get fix on high-shear mixing", *Chem. Eng. Prog.*, **95**: 33 -42.
- Nienow, A. W., 1997. "On impeller circulation and mixing effectiveness in the turbulent flow regime", *Chem. Eng. Sci.*, **52**: 2557 – 2565.
- Ng, K., Fentiman, J., Lee, K. C. and Yianneskis, M., 1998. "Assessment of sliding mesh CFD prediction and LDA measurements of the flow in a tank stirred by a Rushton turbine", *Trans. IChemE, Part A*, **76**: 737 – 747.
- Ng, K. and Yianneskis, M., 2000. "Observations on the distribution of turbulence energy dissipation in stirred vessel", *Trans. IChemE, Part A*, **78**: 334 – 341.
- Pacek, A. W., Chamsart, S., Nienow, A. W. and Bakker, A., 1999. "The influence of impeller type on mean drop size and drop size distribution in an agitated vessel", *Chem. Eng. Sci.*, **54**: 4211 – 4222.
- Padron, G. A., 2005. "Effect of surfactants on drop size distribution in a batch, rotor stator mixer", Ph.D. thesis, University of Maryland, College Park, MD, USA.
- Padron, G. A., 2000. "Measurement and comparison of power draw in rotor stator mixer". M.Sc. Thesis, University of Maryland, College Park, MD, USA.
- Roussinova, V., Kresta, S. M. and Weetman, R., 2003. "Low frequency macroinstabilities in a stirred tank: scale-up and prediction based on large eddy simulations", *Chem. Eng. Sci.*, **58**: 2297 – 2311.
- Shinnar, R., 1961. "On the behavior of liquid dispersions in mixing vessels", *J. Fluid. Mech.*, **10**: 259.
- Versteeg, H. K. and Malalasekera, W., 1995. *An Introduction to Computational Fluid Dynamics :The Finite Volume Method*, Longman Scientific and Technical, Harlow, Essex, England.
- Wu, H. and Patterson, G. K., 1989. "Laser-Doppler measurement of turbulent flow parameters in a stirred vessel", *Chem. Eng. Sci.*, **44**: 2207 – 2221.
- Yeoh, S. L., Papadakis, G. and Yianneskis, M., 2004. "Numerical simulation of turbulent flow characteristics in a stirred vessel using the LES and RANS approaches with the sliding/deforming mesh methodology", *Trans. IChemE, Part A*, **82**: 834 – 848.
- Zhou, G. and Kresta, S. M., 1996. "Distribution of energy between convective and turbulent flow for three frequently used impellers", *Trans. IChemE, Part A*, **74**: 379-389.
- Zhou, G. and Kresta, S. M., 1998. "Correlation of mean drop size and minimum drop size with the turbulence energy dissipation and the flow in an agitated tank", *Chem. Eng. Sci.*, **53**: 2063 – 2079.